Aerogel production by supercritical drying of organogels: experimental study and modelling investigation of drying kinetics

Mouna Lazrag, Cecile Lemaitre, Christophe Castel, Ahmed Hannachi, Danielle Barth

Aerogel production by supercritical drying of organogels: experimental study and modelling investigation of drying kinetics

Mouna LAZRAG[1, 2], Cécile LEMAITRE[1], Christophe CASTEL[1], Ahmed HANNACHI[2], Danielle BARTH[1*]

[1] Laboratoire Réactions et Génie des Procédés, Université de Lorraine, CNRS, LRGP F-54000 Nancy, France
[2]Laboratoire Génie des Procédés et Systèmes Industriels (LR11ES54), Ecole Nationale d'Ingénieurs de Gabés, Université de Gabés, Avenue Omar Ibn El Khattab, Zrig Eddakhlania, 6072, Tunisia

*Corresponding author e-mail: danielle.barth@univ-lorraine.fr
Tel: 33 (0)3 72 74 37 91

Abstract

A supercritical process to dry organogels, in order to produce aerogels is studied. The organogel is firstly produced by synthesizing an amino-acid-type organogelator of fibrillary structure, which is able to trap a solvent, here tetralin. The extraction of tetralin from the organogel using supercritical CO_2 is then investigated both through experiments and simulations. Two approaches are developed in order to understand the tetralin mass transfer mechanisms. In the first approach, the organogel is regarded as an impenetrable material and the mass transfer within it is assumed to be only diffusive. In the second approach, the organogel is considered as a penetrable porous material so that CO_2 can flow across it. The tetralin transfer is thus governed both by diffusion and convection. Both approaches are implemented in Computational fluid dynamics (CFD) software ANSYS Fluent. The drying kinetics obtained by the second approach is found to agree better with the experimental results.

Keys words: Organogel, supercritical drying**,** aerogel**,** diffusion –convection, CFD

1. Introduction

1.1.Processes used to dry gels

The drying of a gel containing a solvent is operated by extracting the interstitial solvent. This process allows to produce a dry material with a highly porous structure and so a low thermal conductivity. Because of the risk of degrading the product solid structure, this operation is delicate. Different drying processes have been developed and used for inorganic gels such as silica gels: freeze drying, evaporative drying and supercritical drying (**Fig. 1**)[1]. Freeze

drying applied to nanostructured silica gels leads to cryogels that are usually cracked and show obvious damages in the pore structure [2]. Evaporative drying is performed at atmospheric pressure and the obtained material is generally called xerogel [3]. Supercritical drying was developped in the 1930's by Kistler [4]. Above the critical point, the sharp distinction between liquid and gas phases disappears, inhibiting surface tension effects which are held responsible for the gel degradation. This technique has proved to be far more efficient and to produce monolithic aerogel materials [1].

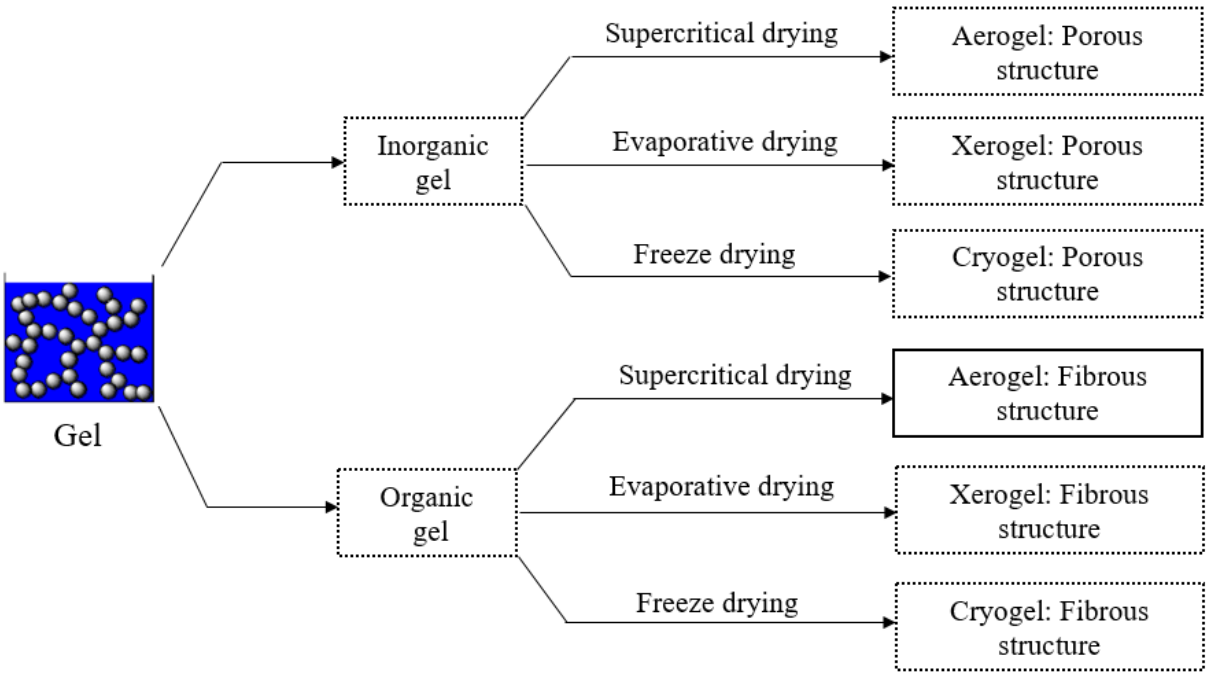

Fig. 1. Methods of gel drying and their outcome [1].

1.2.Structure of the resulting aerogels, xerogels and cryogels

Aerogels are derived from the supercritical drying of two main categories of gels (**Fig. 1**): inorganic gels such as silica aerogels and organic gels, such as the organogels studied in this paper. SEM (scanning electron microscopy) images of xerogels, cryogels and aerogels obtained by the evaporative drying, freeze drying and the supercritical drying techniques respectively were studied in previous works [3,5–8]. The structural patterns are very ramified which allows a low bulk density and a large porous volume in the materials. All aerogels are less dense than xerogels and cryogels. Indeed, aerogel samples display the least shrinkage compared to cryogels and xerogels. Among these materials, aerogels are generally the most porous media and possess the largest surface area [3,7]. Xerogels, cryogels and aerogels produced from silica gels have similar cloudy and diffuse structures, with very small

interconnected units [3,5] . The pores have similar nanometric sizes (generally 1-100 nm) [9,10]. On the contrary, the materials obtained from organogels display highly entangled fibrillar structures, presenting a discontinuous skeleton of fibers with random distribution [6,7]. The aerogel fibers are less thick than the fibers of the materials obtained from the same organic gels but with other drying techniques [7]. Organic aerogels are less fragile than inorganic aerogels [11,12]. It was shown that they can be converted into carbon aerogels through pyrolysis [13].

The first organic aerogels of natural origin and their derivatives were produced by Kistler [4,14]. Resorcinol/formaldehyde (RF) and melamine/formaldehyde (MF) are two of the most common precursor mixtures to form the organic polymer network [15,16]. Organic aerogels are also prepared from cellulose, the most abundant polymer in nature [7,17]. The pore volume fraction of nanofibers at the cell wall of cellulose aerogels has an important influence on the mechanical properties [7]. However, cellulose aerogels display an impact strength much larger than that of RF aerogels and thousand times larger than for inorganic aerogels [17].

The aerogels studied here are obtained from organogels, which can be prepared with different types of solvents. For aerogels produced from toluene and tetralin organogels, with a weight percentage of gelator between 0.5 and 1 mass % introduced in the solvent, the fiber diameters are nanometric in both cases.

1.3.Properties and applications of aerogels produced by supercritical drying

Silica aerogels, the most common and extensively studied aerogels, show outstanding properties such as high porosity (80–99.8%), high specific surface area (500–1200m^2/g), very low conductivity ($<0.02 W.m^{-1}K^{-1}$) [18], low density (~0.003 g/cm^3), low index of refraction (~1.05) and ultralow dielectric constant (k = 1.0–2.0) [19]. Owing to these properties, the aerogels open numerous application perspectives such as acoustic and thermal insulation and to a lesser extent, catalysis, electric devices, filtration and collection devices [20]. The industrial production of aerogels is mainly limited to silica-based systems, carbon, and some small amounts of organic aerogels [21].

1.4. Organogels used to produce aerogels

Organogels are physical organic gels made of a three-dimensional network of gelator molecules, which trap the solvent and prevent its flow. Weak bonds ensure the cohesion of

this supramolecular network. The gelator molecules, also called organogelators, have a low molecular weight (<3000 $g.mol^{-1}$) and can be amino acid derivatives such as phenylalanine, as in the present study. The bonds responsible for the gelation phenomenon in this case are π–π stacking interactions, hydrogen bonding and van der Waals interactions [6, 22-24]. The organogelators show gelation capacity in various solvents such as aromatic solvents (toluene, benzene, tetralin...), alcohols, and ketones. The organogel studied in this paper are produced with tetralin as a solvent.

1.5.Some lessons from previous supercritical gel drying practices

The gel supercritical drying to produce aerogel is based on two crucial steps, the solvent removal from the organogel by supercritical CO_2 extraction and the separation of the solvent-CO_2 mixture. Extraction of the liquid solvent by preserving the gel texture and in particular its original porous network is an important issue in aerogel production. In experimental studies, this step needs to be conducted without creating a liquid-vapor interface, since the resulting capillary forces in the pores cause shrinkage and cracking of the gel samples due to internal stress [25]. According to Novak and Knez [26], the quality and the shape of this kind of aerogels, monolithic cylindrical silica gels formed with methanol, were governed by diffusion of methanol solvent in the CO_2 phase. Furthermore, cracking of samples resulted from rapid drying while transparent crack-free aerogels were obtained for slow drying. Non-transparent areas were observed inside the silica aerogel with intermediate drying times [26].

In order to understand the phenomena occurring within the gels during supercritical drying, the most important parameter to follow is the solvent transport into the porous medium. In the earliest studies, researchers considered that mass transfer was purely governed by diffusion phenomena. For this reason, they focused on the experimental determination of the effective solvent-CO_2 diffusion coefficient through gel structure. In the work of Wawrzyniak [27], this parameter was determined for ethanol-CO_2 at different temperatures and pressures, by combining the diffusional resistances in the fluid phase and structural gel parameters, porosity and tortuosity [27]. The effective methanol-CO_2 diffusion coefficients through cylindrical gels at two different temperatures were also determined experimentally by Novak and Knez [26]. A recent experimental research showed the reliability of NMR (Nuclear Magnetic Resonance) technique in-situ to estimate this parameters at ambient temperature for different methanol-CO_2 and ethanol-CO_2 mixtures within silica gels as a function of the solvent concentration and pressure [28]. Sanz-Moral *et al.* [29] studied experimentally the supercritical CO_2 aerogel drying by image analysis of video captures. Cylindrical silica alcogels produced with

methanol were followed in a high pressure view cell. The mass transfer mechanisms were investigated through analysis of the aerogels transparency evolution during drying. In the early stages of drying, the mass transfer inside the gel was found to be dominated by convection, the drying rate evolution directly depending on the CO_2 flow rate. On the contrary, diffusion governed the transfer of methanol through the alcogel in the later stages [29].

Quiño *et al*. [30] used Raman Spectroscopy to determine the composition of the CO_2/ethanol mixture inside gels during supercritical drying, as a function of time and position. From the obtained CO_2 and ethanol concentration fields, the authors concluded that the ethanol is permanently removed from the structure of the gel while CO_2 travels into and out of the sample at the beginning and at the end of the drying operation, respectively. The diffusion coefficient has been determined as function of CO_2 concentration by fitting the experimental data with the analytical model of Crank [31].

1.6. State of the art on modelling and simulations of gel supercritical drying

In order to model and optimize the supercritical drying process, a good understanding of the phenomena that occur in the complex system of solvent and carbon dioxide is necessary. Process optimization leads to an overall cost reduction and modelling is the key to estimate the drying time and to contribute to the process development. With this respect, different studies can be found in the literature. The systems studied are generally silica gel and an alcohol. A mechanistic model was proposed by Mukhopadhyay *et al.* on supercritical drying of silica aerogel by focusing on mass transfer modeling of CO_2 and ethanol to and from the gel [32]. It was based on the assumption that the pores are parallel arrangements of cylinders. The pore structure was considered open on one or both ends, with direct contact with supercritical CO_2 ($SCCO_2$) at the open end. The diffusive CO_2 flux and the convective mass ethanol flux to and out of the open end of the pores were calculated. The effective diffusion coefficient is introduced as a function of molecular and Knudsen diffusion. The C++ language was used to solve classical mass balance equations of the 1D model. It was concluded that the supercritical extraction of ethanol occurred by spillage due to the supercritical CO_2 dissolution in the pore liquid rather than by the convective evaporation. The drying time was found theoretically to depend strongly on different parameters such as flow velocity of $SCCO_2$, gel thickness, temperature, and pressure. Only the effect of the gel thickness was validated experimentally.

Orlovic *et al.*[33] studied the case of alumina/silica gels containing 1-butanol solvent. They simulated the transfer of the solvent in the gel by pure diffusion. An effective diffusivity was determined with four different models. The two first models were shrinking core models in which a unique effective diffusivity was taken for the whole porous medium. One used Knudsen diffusivity while the other used tortuosity and porosity in the calculation of the diffusivity. The two last models were based on particular pore arrangements. Parallel pore arrangement modeled the simultaneous drying of all pores. Pores in series modelled the successive drying of the pores from the largest to the smallest. A different effective diffusivity was used for each pore size by considering Knudsen diffusion for the micropores. Better fitting of experimental data was obtained for the two last models.

In the theoretical approach of Griffin *et al.*[34], gels of annular geometry and blown around by $SCCO_2$ were modeled with 2D axisymmetric COMSOL model. The mass transfer model considered pure diffusion within the gel. Only molecular diffusion was taken into account and Knudsen diffusion terms were not considered. The gel structure, porosity and tortuosity were assumed not to affect diffusion. The model included a diffusion coefficient dependent on the solvent composition. The results were compared with experimental data obtained from a pilot unit that ensured a continuous measurement of the solvent (ethanol) extraction for different gel thickness and CO_2 mass flow rate. A good agreement was found between theoretical and experimental results. It was also concluded from experiments that the ethanol extraction process is due to sole diffusion phenomena, a significant effect on drying time of both gel thickness and CO_2 mass flow rate was shown.

In the study of Ozbakir *et al*. [35] the mass transfer within the cylindrical gel and in the flowing $SCCO_2$ was modelled. The mass transfer inside the gel was assumed to be diffusive. Mass transfer occurred by convection from the gel surface to the flowing $SCCO_2$ stream. The effective diffusion coefficient for the porous gel was estimated proportional to both the CO_2-ethanol diffusion coefficient and gel porosity and inversely proportional to the gel tortuosity. The binary diffusion coefficient was considered a function of the CO_2 mole fraction. To describe mass transfer along the tubular extraction vessel, a convective mass term was taken into account. Experiments were carried out with a $SCCO_2$ continuous flow surrounding a cylindrical silica gel in a tubular extraction vessel allowing to measure the mass of ethanol removed as a function of time. The gel experimental extraction profiles were compared to the model predictions. A good agreement was reached using mass transfer coefficients fitted from the experiments that varied from an experiment to other. The effect of the CO_2 flow rate on

drying kinetic was studied both experimentally and theoretically. It was concluded that the increase of CO_2 flow rate led to a decrease of effluent concentration at a specific time. However, the effect on the rate of extraction of ethanol was not significant. The simulations were used to investigate the effect of the effective diffusion coefficient and gel thickness. It was found that the drying time of the silica gel decreased with increasing effective diffusion coefficient and decreasing gel thickness. For instance, the solvent concentration was divided by two after 10 min for a diffusion coefficient of 5.10^{-9} m^2/s and after120 min for a diffusion coefficient ten times lower ($0.5.10^{-9} m^2/s$). Also, the drying time increased from 50 min to 300 min when the diameter was increased from 0.5 cm to 2 cm.

Supercritical solvent extraction process was also simulated using CFD (Computational Fluid Dynamics) techniques. Lebedev *et al*. [36] performed simulations to describe the supercritical drying process of silica gels. They developed a mathematical model describing the flow in the reactor of a supercritical alcohol-CO_2 mixture, assumed a compressible viscous fluid. In their approach, heat and mass transfer were also accounted for. ANSYS-Fluent software was used for simulations. Two flow domains were considered in the system: the volume of the porous body (gel) and the free volume of the reactor. In the porous medium, mass transfer was described by Fick diffusion equation accounting for molecular diffusion only. The CO_2-alcohol mixture inside the reactor was described by Peng-Robinson equation of state. The experimental study of the supercritical drying kinetics was performed with ten cylindrical monolithic gels. The developed model represented adequately the experiments. The influence of flow rate and gel thickness on kinetic curves was investigated showing a significant effect.

In almost all the previous researches, the dried gels were silica gels. Very few papers treated the case of organic gels. Garcia-Gonzalez *et al*.[37] have studied the supercritical drying of gels from different precursors (inorganic silica gel and organic starch gels) in order to show the precursor effect on the kinetics profile. The solvent (ethanol) removal process was followed experimentally. The solvent extraction was studied experimentally by measuring its amount in the CO_2 gaseous stream, using an alcoholmeter device. It was concluded that the gel supercritical drying is governed by a mass transfer mechanism based on a combination of both convection and diffusion inside the gel. In the first drying step (0-60% of recovery rate), convective mass transfer was shown to play a significant role while the last drying step is controlled by diffusion. The experimental drying profiles were compared to theoretical profiles calculated considering only Fickian diffusion-based model without convective transport. This model failed to predict correctly the experimental data. The effective diffusion

coefficient was determined by using the curve fitting Matlab tool. The obtained values were slightly higher than those found in the previous literature for the silica aerogel (10^{-8} m^2/s). The effective diffusion coefficient of organic starch aerogel were almost ten times lower than that found for the monolithic silica aerogel (10^{-9} m^2/s). This last value is the only value found in the literature for organic gels. The drying profiles of inorganic silica gel and organic starch gels were compared to investigate the effect of precursor nature of the gel. It was found that both drying profiles followed a similar two-step drying rate behavior. However, the drying rate was lower in the case of organic gel. The authors attributed this to the difference between the gels textural properties which could affect the diffusion process. Moreover, they assumed that the interaction of ethanol with the starch components of the organic gel might hinder and delay the solvent extraction. The effect of morphology in the drying process was also studied by comparing the experimental drying profiles of cylindrical monoliths and microspheres gels having the same target densities. It was observed that these profiles were similar in the first drying step (0-60% of recovery rate) then the drying process of microspheres was faster than for the cylindrical monoliths. This was explained by the threshold point at which the drying process became more affected by the diffusion phenomena. The minimum diffusion path length was shown to have a significant effect on the drying process by comparing organic gels profiles with different geometrical shapes (cube and cylinder) and sizes.

So far, most models reported in the literature describe the supercritical drying of inorganic silica gels (**Table 1**). The present study focuses on the supercritical drying of organic gels, derived from a low molecular weight molecule, which have been received little attention. The structure and properties of aerogels derived from organogels are very different from those derived from silica gels. Furthermore, the solvents used to produce silica gel were often alcohols like ethanol, methanol and isopropanol. The solvent chosen here is tetralin, which is aromatic and not volatile. At the best of our knowledge, it was never used in the past to produce gels. A new theoretical approach is developed in this paper in order to model the supercritical drying of organogels accounting for diffusion as well as convective mass transfer. In fact, two different approaches are assumed and compared, depending on the penetrable or impenetrable nature of the organogel.

248

249 **Table 1**. Models describing supercritical drying of gels in literature and in the present paper

Gel nature	Mass transport in sample	Diffusivity determination in sample	Mass transport in surrounding fluid in autoclave	Software & geometry	Reference
Inorganic	-Simulation of one pore, -Diffusion only - Boundary condition: convection at the end of the pore	-Effective diffusivity function of molecular and Knudsen diffusion - Molecular diffusivity in CO_2 dependent on solvent concentration	Not considered	- C++ - 1D model	[32]
Inorganic	-Diffusion only -Boundary condition: constant concentration at the sample surface	Effective diffusivity: 4 different models dependent on molecular diffusivity in CO_2, porosity and tortuosity and Knudsen diffusivity	Not considered	- Fortran - 1D model	[33]
Inorganic	Diffusion only	Molecular diffusivity in CO_2 dependent on solvent concentration	Convection-diffusion	-COMSOL -2D axisymmetric simplified model	[34]
Inorganic	Diffusion only	- Effective diffusivity calculated as function of molecular diffusivity and tortuosity and porosity - Molecular diffusivity in CO_2	Convection-diffusion	- Matlab -2D axisymmetric model	[35]

		dependent on solvent concentration			
Inorganic	Diffusion only	Molecular diffusivity in CO_2 dependent on solvent concentration	Convection-diffusion	- Ansys-Fluent -3D geometry	[36]
Inorganic/ organic	-Diffusion only -Boundary condition: zero concentration at the sample surface	Fitted effective diffusivity	Not considered	- Matlab -Analytical 1D model	[37]
Organic	Diffusion Only	Effective Diffusivity Calculated by a correlation from litterature	Convection-diffusion	- Ansys-Fluent -3D model	Present paper Approach 1
Organic	Convection-Diffusion	Calculated Molecular diffusivity in CO_2 by an equation from litterature	Convection-diffusion	- Ansys-Fluent -3D model	Present paper Approach 2

2. Experimental drying of cylindrical organogels

In this section, a drying experiment of organogels is described and kinetic results are presented.

2.1. Organogel preparation

The process to obtain organogel is based on two main steps. The first step is the synthesis of low molecular weight organogelator molecules derived from amino acids (Phenylalanine Phe) which was described by Brosse *et al.*[22]. It consists of an esterification of the Z group (benzyloxycarbonyl) protected amino acid, called Z-Phe-OMe, followed by a hydrazide synthesis (Z-Phe-NH-NH_2) by reacting the ester with hydrazine hydrate. Then, the final compound, the organogelator (Z-Phe-NH-Napht) is obtained by condensation of naphthalic anhydride with the hydrazide. The second step consists in the gel formation by dissolving and stirring a desired amount of the organogelator into a desired amount of organic solvent (here tetralin) in a round bottomed flask connected to a reflux condenser at T=80°C. The hot solution is then transferred into a cylindrical mold and cooled down to T= 4°C [6]**.** Four cylindrical organogel samples with 30 mm diameter and 6.7 mm, 10.5 mm, 10.5 mm and 12.9 mm height respectively were prepared following this experimental protocol.

2.2. Experimental setup for organogel drying

The organogels drying is carried out in a home-made supercritical laboratory equipment represented in **Fig.2**. This unit is mainly composed of a high pressure cylindrical extractor or autoclave[9] of 250 ml volume where the organogel is dried. Gaseous CO_2 (50-60 bar) supplied by a CO_2 bottle[1] is liquefied by cooling in a cold exchanger[2] at 4°C. A pump[4]manufactured by LEWA (EK1) pushes the liquid CO_2 into the back pressure regulator[6]. The pressure of the CO_2 leaving the pressure regulator is 180 bar. Then, it is heated in a hot exchanger[7]up to 45°C. Under these conditions (45°C and 180 bar), the CO_2 flow is under supercritical state. The autoclave containing the gel is fed with the supercritical CO_2. The organogel sample is placed on a bed of glass beads (**Fig. 3**). The CO_2 entering from the bottom of the autoclave first flows through this bed before it is blown around the sample. The cumulative mass and the flow rate of CO_2 are measured using a Micromotion[8]Coriolis mass flowmeter placed upstream from the autoclave with $\pm 1\,g$ accuracy. The pressure inside the autoclave is controlled by a pressure gauge (PI1).The supercritical CO_2 allows organogel drying by extracting the tetralin from its porous structure. The CO_2-tetralin mixture leaving the autoclave is then separated in a cascade of three successive separators[10]operating at 50 bar, 30

bar and atmospheric pressure respectively and at 20°C. Further details about the drying process and the separation are provided in [38].

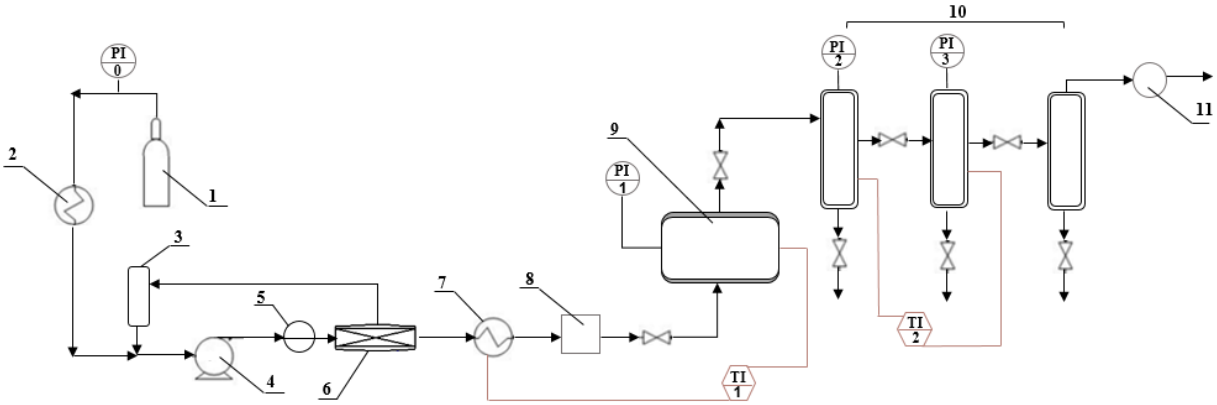

Fig.2. Scheme of the supercritical drying set-up: 1-CO_2 bottle; 2-cold exchanger; 3-CO_2 tank 4-pump; 5- Damper, 6-back pressure regulator; 7-hot exchanger; 8-Coriolis mass flowmeter; 9-autoclave; 10- three cyclone separators; 11- Flowmeter, PI-pressure gauge, TI-thermostatic bath.

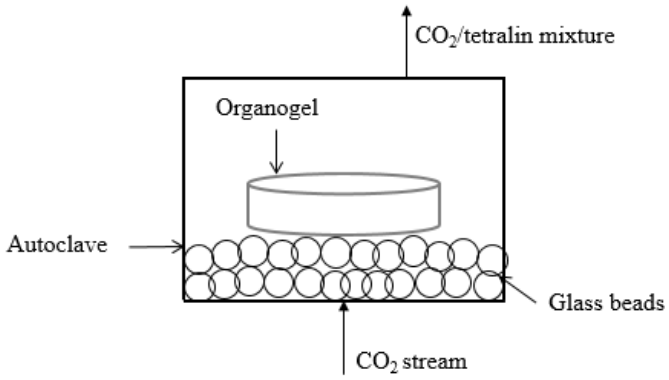

Fig. 3. Organogel sample placed in the autoclave

2.3.Drying procedure

The organogel drying procedure in order to obtain the aerogel follows several steps, during which the temperature and pressure in the autoclave evolve with time, as described in **Fig. 4** and detailed hereafter:

- Step 1: autoclave filling with CO_2 for 15 min
- Step 2: pressurization of the autoclave for 20 min up to 180 bars
- Step 3: autoclave heating for 20 min up to 45 °C
- Step 4: supercritical extraction by transport of tetralin from the gel to the CO_2 stream

- Step 5 and 6 : depressurization and decrease of temperature to the ambient conditions during 30 min

At the end of these steps, the autoclave is opened and the aerogel is recovered.

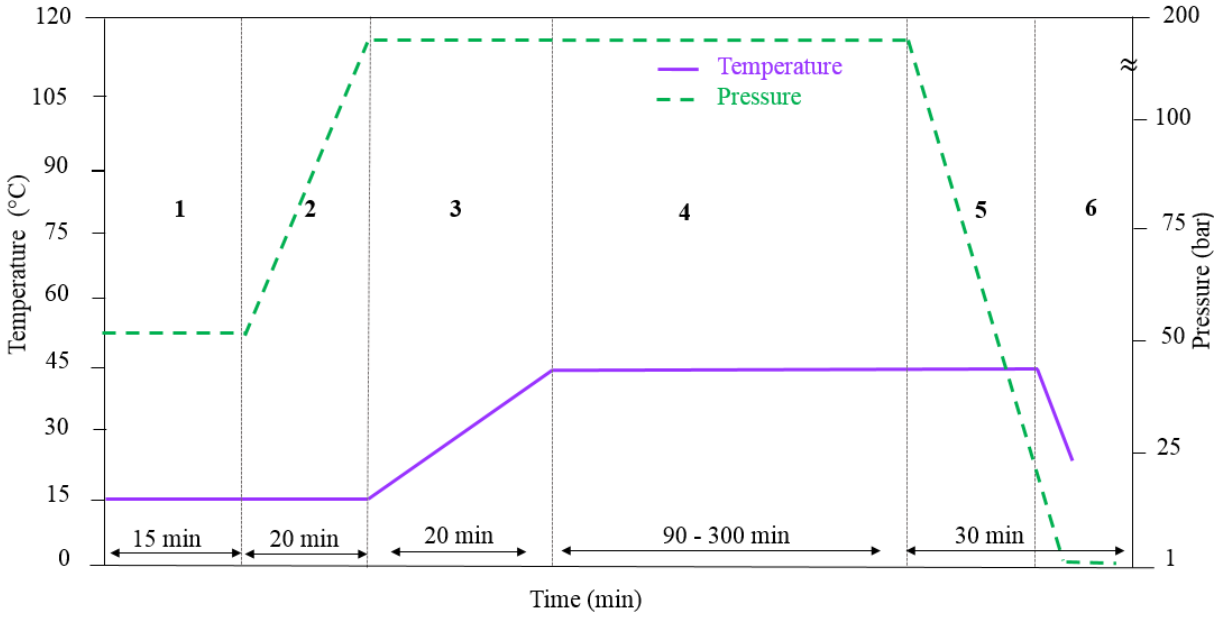

Fig. 4. Steps of drying in the autoclave: temperature and pressure enforced in time.

The step of supercritical extraction is the crucial and the longest step. During this step, the liquid phase is collected every 15 min from the bottom of the separators and then weighed ($\pm 0.1 mg$). The weight values are summed up and the total quantity of tetralin recovered from the autoclave during the supercritical extraction is determined. The CO_2 flow rate slightly varies along the extraction process. However, instantaneous flow rate measurements, showed that the variations did not exceed 10 %. The pressures in the separators are regulated manually by depressurisation valves and also recorded at each collecting step. At the end of supercritical extraction, the mean CO_2 flow rate is calculated as the arithmetic average of the measured flow rates.

The sample thickness and the CO_2 flow rate differed for every experiment. This is why it was not possible to perform replication tests.

2.4.Drying experiments results

The four cylindrical samples with different size described in section 2.1 are dried according to this experimental protocol. The experimental data and results, gel thickness, organogelator weight fraction, tetralin mass in the gel, mean CO_2 flow rate, drying time, initial tetralin

concentration, and tetralin degree of recovery, are reported in **Table 2**. The initial tetralin concentration is calculated as the ratio of the tetralin mass in the gel to the pore volume of the sample, multiplied by the tetralin molar mass. The experimental tetralin degree of recovery is the ratio of the total quantity of tetralin recovered from the autoclave to the initial total quantity of tetralin in the gel. The final recovery is satisfactory, around 90% but is not complete (**Table 2**). A thermodynamic modeling of CO_2/tetralin separation has been carried out and the tetralin degree of recovery has been computed in a former work [39] .

The computed recovery (theoretical tetralin recovery) were in agreement with the experimental values (experimental tetralin recovery). The discrepancies may be attributed to experimental errors and to variations of CO_2 flow rate and pressures during experiments. In the thermodynamic model, on the contrary, the flow rate and the pressures are assumed constant all along the experiments.

The unrecovered amount is due to thermodynamic reasons: about 10% of the tetralin stays in the gas phase and leaves the separators with the CO_2 through the upper gas exits, as explained by Lazrag *et al*.[39].

Table 2. Experimental data and results of the four organogel samples

Sample	**Exp.1**	**Exp.2**	**Exp.3**	**Exp.4**
Gel thickness (mm)	6.7	10.5	10.5	12.9
Organogelator weight fraction (%)	1	1	1	0.5
Tetralin mass in the gel (g)	4.500	7.086	7.075	8.735
Initial tetralin concentration (mol.L^{-1})	7.409	7.445	7.443	7.470
CO_2 mean flow rate (g/h)	729	733	820	540
Drying time (min.)	150	240	240	240
Experimental tetralin degree of recovery (%)	81	91	88	87
Theoretical tetralin degree of recovery (%)	89.0	85.9	85.9	92.3
Mean tetralin molar fraction (%)	0.09	0.07	0.07	0.13

To compare the experimental results with the numerical calculations presented later, the instantaneous recovery rate is considered relatively to the recovered value at long times,

$$\text{NTRR} = \frac{\text{tetralin cumulative quantity recovered at a time t}}{\text{tetralin total quantity recovered from the autoclave}} \qquad (1)$$

and is called the normalized tetralin recovery rate (NTRR). In **Fig. 5**, the experimental NTRR is presented as a function of time.

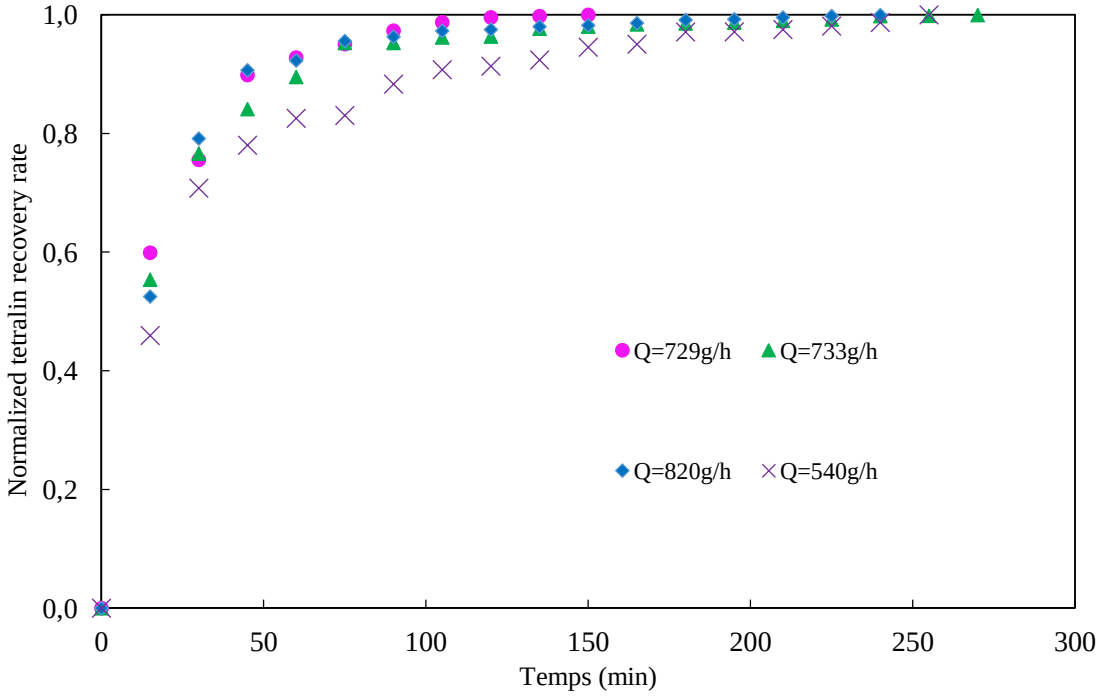

Fig. 5. Experimental supercritical drying kinetics of the four organogel samples

As stressed before, the normalized tetralin recovery rate considers the total cumulative solvent quantity and not the initial quantity of the solvent in the gel as the reference, thus leading to 100% recovery rates for all four experiments. The experimental drying time differs from one experiment to another and ranges between 150 and 240 min. In section 3, a theoretical study is conducted to model the drying kinetics. Two different models are developed depending on the mass transfer mode inside the gel volume, whether governed by diffusion-convection transport or only by Fickian diffusion.

3. Mathematical models and simulation results

3.1. Thermodynamics Data

As explained in section 1, supercritical monophasic conditions are enforced in order to obtain a well-dried and non-cracked aerogel. In all studied experiments (Table 1), the tetralin concentration does not exceed 1% (mol). In **Fig. 6**, the equilibrium diagram of the CO_2-tetralin binary mixture is presented at two temperatures (40°C and 71°C), between which lies the actual autoclave temperature of the drying process (45°C). The experimental bubbles and dew points were taken from the literature and were summarized in a previous work [23]. The theoretical curves were determined from a thermodynamic model detailed in the same paper. This diagram shows that the selected experimental conditions, 45°C and 180 bar with a tetralin molar fraction inferior to 0.01 (CO_2 molar fraction > 0.99) produce a supercritical

binary mixture. At these low tetralin concentrations, there is no risk of the appearance of a liquid-vapor equilibrium. As a result, there is no evaporation phenomenon, the resulting mixture is monophasic.

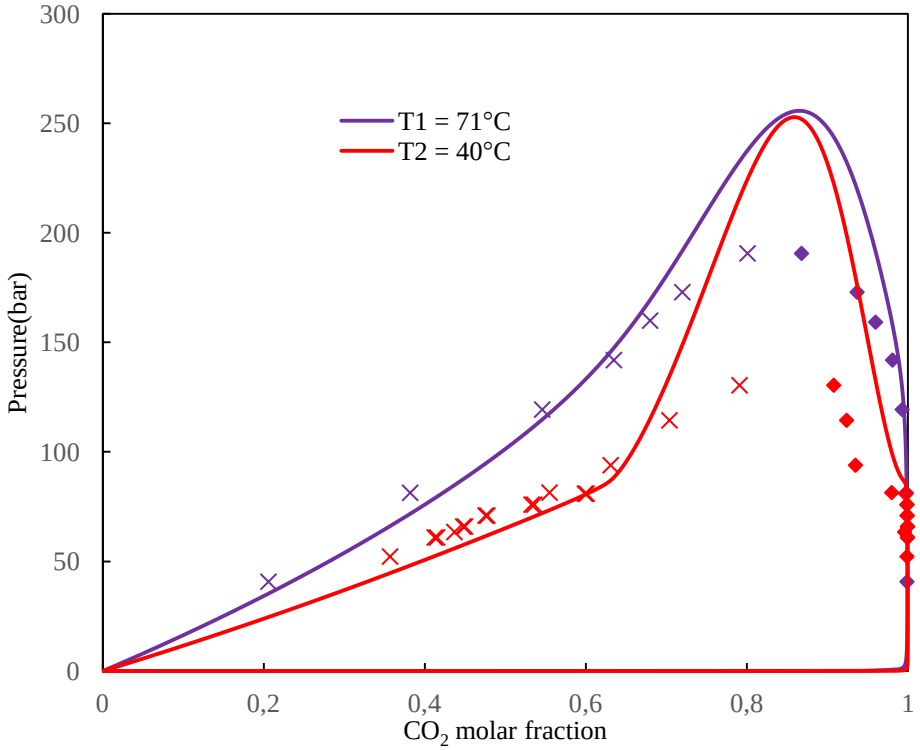

Fig. 6: × experimental bubble points, ♦: experimental dew points.
Solid line: predicted curves with the PPR model [23] for the system CO_2-tetralin at two temperatures : 40°C and 71°C

3.2. Mathematical models

In this modeling study, the system is the organogel sample and the autoclave. The mathematical models are developed to describe the flow hydrodynamics of the supercritical fluid ($SCCO_2$) in the autoclave and the mass transfer of tetralin during the organogel drying process. This model is based on equations of continuum mechanics. The system is divided into three zones: the upper autoclave volume surrounding the sample, the gel volume, and the inferior autoclave volume containing the glass beads.

The produced aerogels samples possess a very high porosity (void fraction) with an average value of 0.97, determined from SEM images [40]. For this reason, an important issue is discussed here, which is to investigate whether the gel sample is penetrable to the CO_2 flow or

not. Two approaches are therefore considered here. In the first approach, the organogel is assumed to be an impenetrable solid. In the second one, the organogel is regarded as penetrable. Both approaches are implemented in Computational fluid dynamics (CFD) software ANSYS Fluent.

3.2.1. Model equations

3.2.1.1. Approach 1: Organogel sample as an impenetrable solid (Pure diffusion transfer inside the gel)

In this approach, the organogel is considered as an impenetrable solid meaning that the surrounding fluid cannot pass through it. The considered assumptions are as follows:

- The flow of the supercritical CO_2 in the free volume is considered laminar ($Re < 60$) and is described by Navier–Stokes equations. Due to the low velocities involved, the Mach number is inferior to 0.3 and the flow may be considered incompressible.
- The inferior volume of glass beads is described as a homogeneous porous medium and the CO_2 flow is governed by Darcy law.
- Tetralin mass transfer in the porous medium of the gel volume is described by Fick's diffusion equation without convective transport. An effective diffusion coefficient is considered, taking into account the porous structure of the gel.
- The system is assumed to be isothermal and isobaric, since it is the case in the experiments, which leads to a constant fluid density.

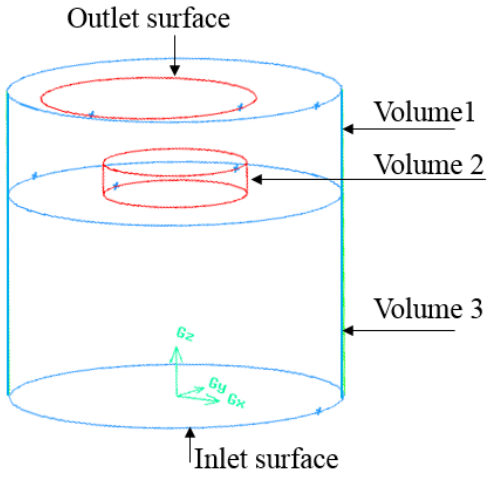

Fig. 7. Sketch of the modeled flow and transport domain. Volume 1: free volume above the sample. Volume 2: organogel sample. Volume 3: Glass beads supporting the sample.

The equations describing the tetralin mass transfer and the hydrodynamics of CO_2 flow in the different autoclave sub-domains (**Fig. 7**), deriving from these assumptions are as follows:

- Model equations in Volume 1, the free upper volume of the autoclave

$$\begin{cases} div(\boldsymbol{v}) = 0 \\ \rho\left(\dfrac{\partial \boldsymbol{v}}{\partial t} + \boldsymbol{v}.\nabla \boldsymbol{v}\right) = -\nabla p + \mu\nabla^2 \boldsymbol{v} + \rho \boldsymbol{g} \\ \dfrac{\partial(\phi)}{\partial t} = \nabla.(D_{AB}\,\nabla\,\phi) - \nabla.(\boldsymbol{v}\phi) \\ \rho = \rho_{CO_2} \end{cases} \quad (2)$$

- Model equation in Volume 2, the organogel sample

$$\frac{\partial \phi}{\partial t} = \nabla.(D_{eff}\Delta\phi) \quad (3)$$

- Model equations in Volume 3, the bottom zone of the autoclave containing glass beads

$$\begin{cases} div(\boldsymbol{v}) = 0 \\ \nabla p = -\dfrac{\mu\,\boldsymbol{v}}{\alpha_b} \\ \dfrac{\partial(\phi)}{\partial t} = \nabla.\left(D_{AB}\,\nabla\,\phi\right) - \nabla(\boldsymbol{v}\phi) \end{cases} \quad (4)$$

where v is the CO_2 velocity, ρ_{CO_2} is the CO_2 density, p is the pressure in the autoclave, g is the gravity constant, ϕ is the mass fraction of tetralin and μ is the CO_2 dynamic viscosity.

The fluid velocity at the walls is zero, i.e. no-slip boundary conditions. Tetralin flux at the walls is also set to zero. There is no tetralin in the CO_2 flow entering the autoclave.

At initial time, the CO_2 fluid around the gel is free of tetralin. The sample contains only tetralin with a uniform molar concentration as described in **Table *2***.

The permeability α of the glass beads bed is estimated with Kozeny-Carman equation [41]:

$$\alpha_b = \frac{d_b {\varepsilon_b}^3}{36\,K_0\tau^2\,\left(1-{\varepsilon_b}^2\right)} \quad (5)$$

where d_b is the glass beads diameter here equal to 10 mm, ε_b is the porosity of random stacking of monodisperse spheres, $K_0\tau^2$ is the Kozeny coefficient that is equal to 4.17, K_0 is the form factor which is equal to 2 for a spherical packing yielding $\tau^2 = 2.085$, where τ is the tortuosity of the glass beads bed [42–44].

The molecular diffusion coefficient D_{AB} is the diffusion coefficient of tetralin (A) in supercritical CO_2 (B). In the literature [45], this coefficient was determined at temperature and pressure conditions different from supercritical drying conditions in this process. It is equal to

1.741 x 10^{-3} cm^2/s at 573 K and 8.97 MPa, and 2.221 x $l0^{-3}$ cm^2/s at 648 K and 8.97 MPa. The hydrodynamic theory of Stokes-Einstein was used by Medina [46] to calculate the diffusivity in supercritical fluids and gave acceptable agreements with experiments. This model assumes the diffusion of large molecules of solute through a continuum of smaller molecules of solvent which seems relevant here considering that the CO_2 molecules (the solvent) are smaller than the solute molecules (tetralin). For this reason, this model is adopted here to estimate the diffusion coefficient D_{AB}:

$$\begin{cases} D_{AB} = \dfrac{k\,T}{6\pi\, r_H \mu_B} \\ r_H = 3.18 \times 10^{-10} (R_A^{vdW})^{1/3} \\ R_A^{vdW} = \dfrac{V_{wA}}{15.17 \times 10^{-6}} \end{cases} \quad (6)$$

Where T is the temperature, k is the Boltzmann constant, μ_B is the viscosity of the solvent, here CO_2, r_H is the hydrodynamic radius of solute A, R_A^{vdW} is the van der Waals volume parameter and V_{wA} is the van der Waals volume of solute A (tetralin).

The organogel sample is considered as homogenous solid within which tetralin diffuses. The free mean path of the tetralin molecules is increased since they must circumvent the gel fibers, which contributes to slow down their motion and is taken into account in the effective coefficient D_{eff}.

Several models have been established for a long time in order to predict the diffusion of solutes in liquid fluids and supercritical fluids [46]. The determination of the diffusion coefficient of a solute in a solid matrix such as solid polymers and gels was also addressed in the literature in order to understand these complex systems from the point of view of mass transfer. Different mathematical models describing the retardation of solute diffusion within gels have been developed which were based on different theoretical approaches. A very good overview of these different theories is given in the literature review of Amsden [47] and Masaro *et al.* [48]. In the present paper, we are concerned by the theoretical approach of obstruction that focuses on gels of fibrillar structure. The presence of impenetrable fibers leads to an increase in the path length for diffusive transport. The fibers, in models based on this theory, are assumed to be at rest and randomly embedded. In this theoretical approach, the greatest importance is given to the structural description of the system. For this reason, the decrease of the diffusion coefficient is correlated with the solute size and the volume fraction of the fibers [29]. Among these models, the one proposed by Ogston [49,50] is selected to

predict the effective diffusivity D_{eff}, diffusion coefficient of the solvent in the supercritical fluid through the matrix of the gel. It allows to predict the ratio D_{eff}/D_{AB} from the structural data on the solute and the gel matrix for the fibrous medium. The Ogston model is usually adopted for fibrous matrix and for random distribution of fibers inside the gel [49,50]. This model describes the repartition of spaces inside a fiber suspension which structure can be compared to that of organogels. The assumptions of this model were the following: the fibers were considered rectilinear and the solute was considered rigid and spherical. The Ogston model is a phenomenological approach where the solute diffusion is the result of random successive movements. This model is chosen in this study to predict the ratio D_{eff}/D_{AB} and the free mean path is taken as the average distance between the organogel fibers. It is expressed in equation (7) as a function of the fiber radius (r_f), the solute hydrodynamic radius (r_H) and the fiber volume fraction (Φ_p), which is equal to $1-\varepsilon$, with ε the gel porosity.

$$\frac{D_{eff}}{D_{AB}} = exp\left[-\frac{r_H + r_f}{r_f}\sqrt{\Phi_p}\right] \quad (7)$$

The calculated effective diffusion coefficient is equal to 4.8×10^{-9} m^2/s (Table 2). This value is close to that found by fitting in the work of Garcia-Gonzalez [37] for organic aerogels which equals to 1×10^{-9} m^2/s.

3.2.1.2. Approach 2: Organogel sample as a penetrable solid (diffusion-convection transfer inside the gel)

In this approach, the organogel sample is assumed to be a penetrable solid allowing the CO_2 to flow through its pores. In this approach the free volume surrounding the gel and the glass beads volume are treated the same manner as in the 1st approach. But the organogel sample is treated as a volume of porous medium. The convective transport is added to molecular diffusion in this medium. The CO_2 flow is governed by Darcy law. In this approach, equation (2) is kept for Volume 1 and equation (4) for Volume 3. But in Volume 2, the organogel sample, equation (3) is replaced by

$$\begin{cases} div(\boldsymbol{v}) = 0 \\ \nabla p = -\frac{\mu\,\boldsymbol{v}}{\alpha_b} \\ \frac{\partial(\phi)}{\partial t} = \nabla.\left(D_{AB}\,\nabla\,\phi\right) - \nabla(\boldsymbol{v}\phi) \end{cases} \quad (8)$$

The permeability α of the fibers bed is calculated using the expression proposed by Davies [51] :

$$\alpha = \frac{{d_f}^2}{64\,(1-\varepsilon)^{3/2}(1+56(1-\varepsilon)^3)} \quad (9)$$

where d_f is the fibers diameter and ε is the organogel porosity, which are measured through SEM images. The values of the different parameters used in these models are reported in **Table 3**. Since the tetralin molar fractions are very low (below 0.13%), the considered density and viscosity are those of pure CO_2. Furthermore, the diffusivities were assumed to be independent of tetralin concentration.

Table 3. Parameter values used in the simulations

Parameter	Value	Reference
ρ (CO_2) (kg.m^{-3})	772.86	[52]
μ (CO_2) (Pa.s)	6.95×10^{-5}	[53]
V_{wA} (cm^3/s)	80.98	[54]
r_H (Å)	5.49	-
D_{AB} (m^2/s)	6×10^{-9}	-
d_f (nm)	207	[40]
D_{eff} (m^2/s)	4.8×10^{-9}	-
ε_b (m^2)	0.39	[55]
α_b (m^2)	10^{-7}	-
ε	0.97	[40]
α (m^2)	1.29×10^{-13}	-

3.2.2. Simulation methods

3.2.2.1.Numerical schemes

In ANSYS-Fluent, the convective terms are discretized using the second order upwind approach. The interpolation model is maintained for the pressure term. In order to solve the transport equation of tetralin, the first order upwind scheme is selected.

3.2.2.2.Computational mesh

The software Gambit is used to create the computational domain and the mesh shown in **Fig. 8**. The mesh is three-dimensional (3D). The domain is divided into three volumes:

- Volume 1, the upper free volume surrounding the sample is discretized with tetrahedral elements
- Volume 2, the organogel sample is meshed with tetrahedral elements.
- Volume 3, the lower autoclave volume that contains glass beads is discretized with hexahedral elements.

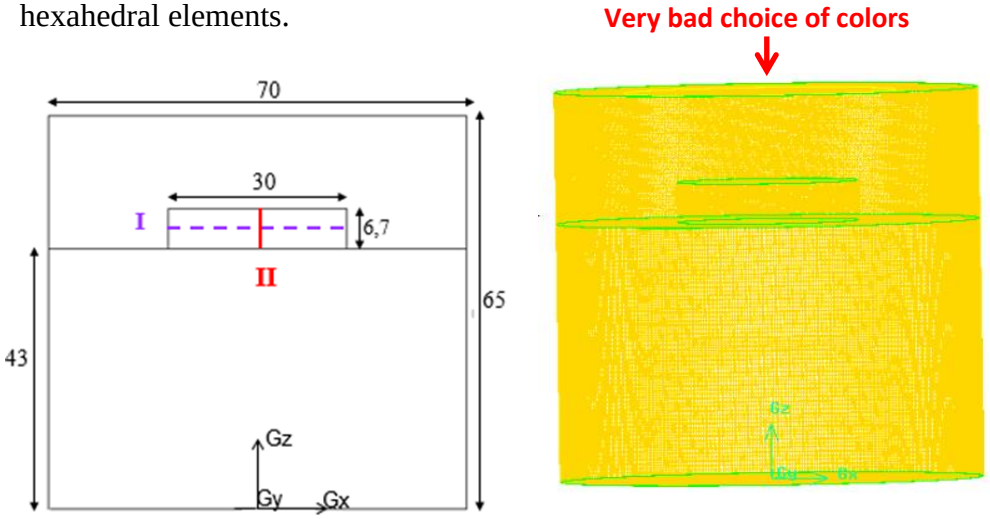

(a) **(b)**

Fig. 8. (a) System dimensions (mm) and segments **I** and **II** used for plotting concentration profiles, (b) Mesh

3.2.2.3.Boundary conditions

The CO_2 velocity is imposed at the autoclave inlet and no-slip conditions are applied at the solid walls.

3.2.2.4.Mesh independence test

The first experiment corresponding to sample 1, of 6.7mm thickness, is chosen as a reference to build the mathematical models. The other experiments (sample 2, 3, and 4) will be compared to theory in a second step. In order to perform mesh independence tests, two meshes are created, a coarse and a refined mesh composed of 3.3 million and 6.5 million cells respectively. In **Fig.9**, tetralin mass fraction profiles in volume 2, the organogel sample, are compared for both meshes with the first approach. These profiles are plotted along two segments, I and II, indicated in **Fig. 8 (a)** and at four different times t=100s, t=500s, t=1500s and t=3000s. As shown in **Fig.9 (a)** and **Fig.9 (b)**, the profiles for both tested meshes, coarse and refined are completely superimposed. This result proves that both meshes are sufficiently refined to ensure a mesh independent solution. The coarser mesh (3.3 million cells) is thus

retained for the calculations in order to reduce the computational efforts. It is noted that the axial profiles are not symmetrical (**Fig.9** (b)) with respect to the plane $z = e/2$ (with e the gel thickness) and that this asymmetry is accentuated over time. The reason is that the convective flux leaving the gel is different on the 3 gel boundaries.

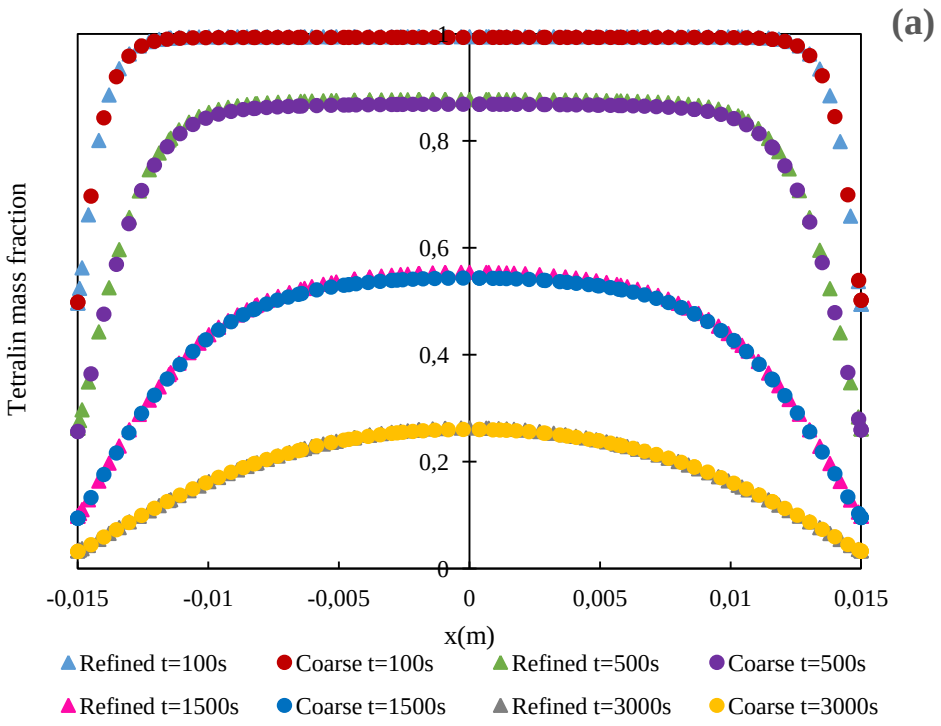

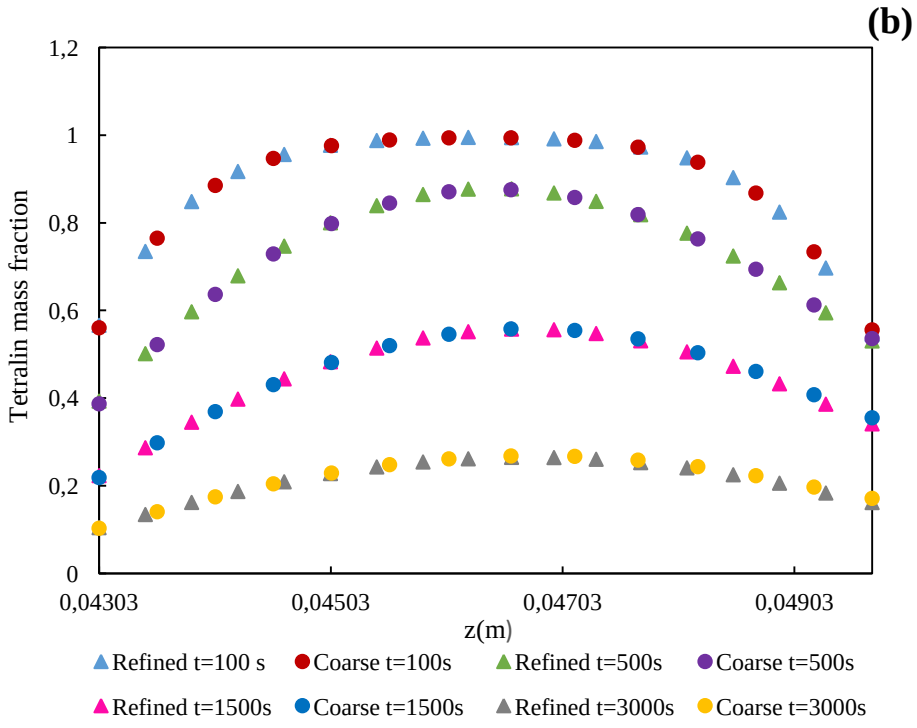

Fig.9. Mesh independence tests: Comparison of the tetralin mass fraction profiles in the organogel sample, obtained with the first approach for two meshes (coarse and refined).
(a) In the radial direction of the gel, along segment I
(b) in the axial direction of the gel, along segment II.
Segments I and II are defined in **Fig. 8**.

3.3. Supercritical drying simulation results

3.3.1. Comparison of the models results

The calculations provide the tetralin mass fraction ϕ inside the organogel sample as a function of time. The theoretical tetralin recovery rate (TRR) extracted from the pores at the drying conditions mentioned in section 2 is also predicted using the following equation

$$TRR = 1 - \frac{\iiint \rho_t \times \phi}{Initial\ Mass\ of\ tetralin\ in\ the\ sample} \quad (10)$$

where ρ_t is the total density and ϕ is the tetralin mass fraction

Both simulations are carried out with a time step $\Delta t = 50$ s which is equal approximately to a thousandth of the characteristic diffusion time computed from approach 1.

$$t_{car} = R^2/D_{eff} = 46\,875\ s \quad (11)$$

The theoretical tetralin recovery rate is computed with the two approaches described in sections 3.1.1. In **Fig. 10**, the models results are compared to the experimental extraction profiles given in **Fig. *5***. A large amount of tetralin is collected in the initial period of the experiment. An extraction rate (amount of tetralin extracted per unit time) of 75% is reached between 25 and 30 min for all experiments, **Fig. 10(a-d)**. The extraction rate decreases with drying progress. The two theoretical drying kinetics are close but the kinetics predicted by approach 2 is closer to the experiment. The discrepancies between theory and experiment are quantified by the least square method and are equal to and 9.4% and 5.6% for approaches 1 and 2 respectively, in the case of the first experiment, **Fig. 10(a)**. For the other experiments 2, 3, and 4, the discrepancies between approach 2 and the experiments are equal to 16%, 19.6% and 16.6% respectively. While, the discrepancies between approach 1 and the experiments are equal to 31.1%, 34.8% and 30.1% respectively. So, the second approach can be considered the closest approach to the experimental reality. The gel appears to behave as a penetrable porous medium. The fibers are not an obstacle against the penetration of fluid. Accordingly, the fibrous matrix of the gel can be assimilated to a sieve in which the solute can diffuse freely.

In this fibrous organogel, it is possible that penetration velocity is not sufficient which can explain the difficulty to discriminate the drying kinetics given by both approaches. But approach 2, which considers the organogel as a penetrable solid allows to represent in a satisfactory manner all the carried out experiments. The deviations, not exceeding 20%, can be explained by the following facts:

- The CO_2 flow rate was not perfectly stable during the experiments while an average constant flow rate was used in the simulations.
- In the theoretical approach, the organogel is considered as a penetrable porous medium. The porosity and permeability values of each organogel sample were unknown and estimated mean values were used for all calculations and simulations.
- In the literature, experimental data corresponding to the molecular diffusion coefficient of tetralin in CO_2 could not be found for the actual operating conditions. The Stokes-Einstein equation used for supercritical fluids was selected to predict the binary diffusivity.

A parametric study on the operating conditions of the supercritical drying, like CO_2 flow rate and organogel thickness, is necessary to show the sensitivity of the drying kinetic with these parameters and may also allow to differentiate the approaches.

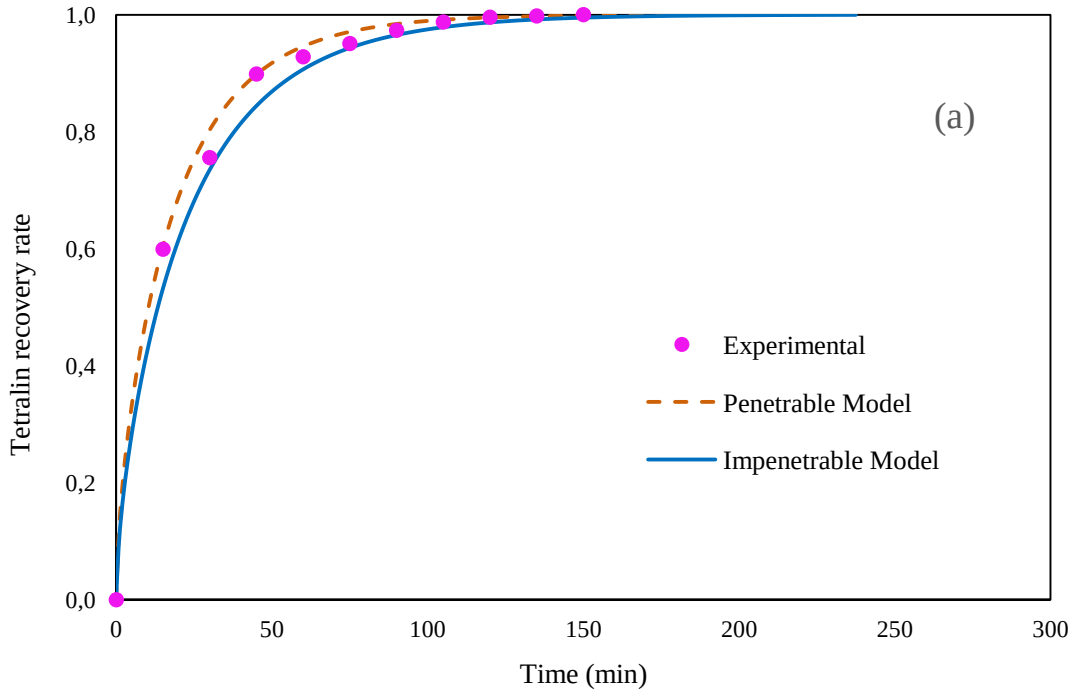

571

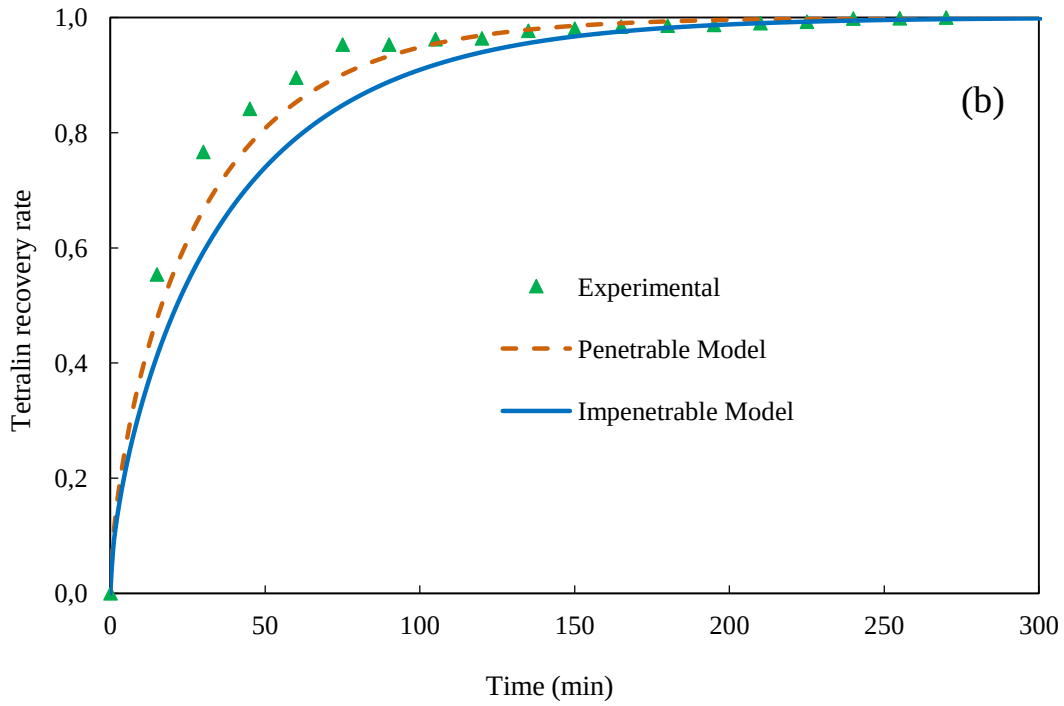

572

573

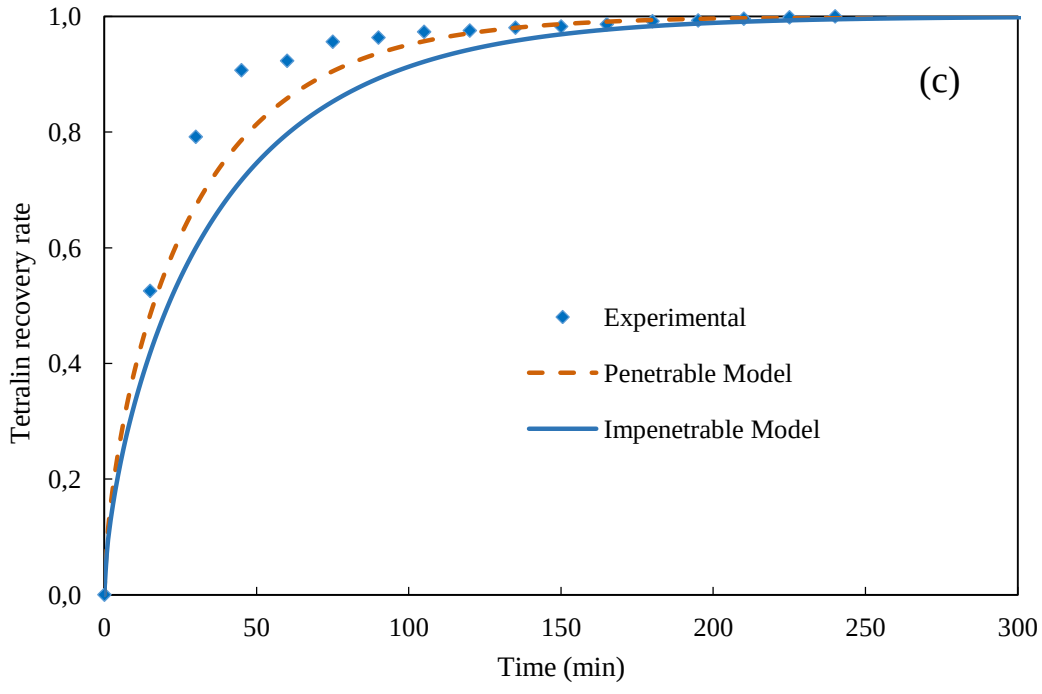

574

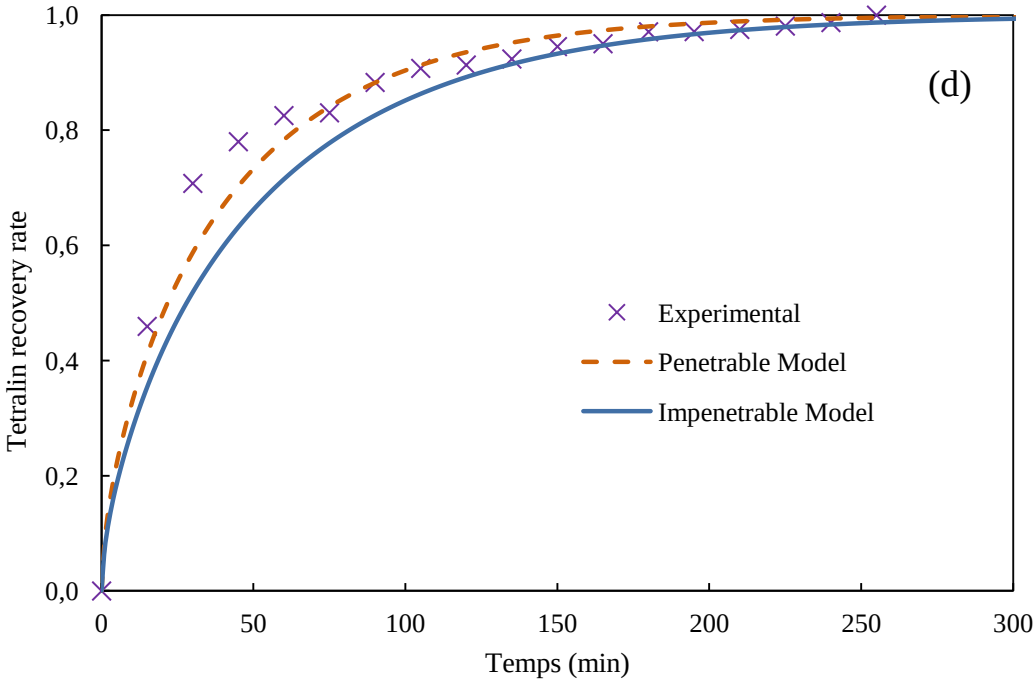

Fig. 10. Comparison of experimental drying kinetics to model results at 180 bar and 45°C (approach 1: impenetrable solid, approach 2: penetrable solid)
(a) Experiment 1: Q=729g/h and e=6.7mm. (b) Experiment 2: Q=733g/h and e=10.5mm.
(c) Experiment 3:Q=820g/h and e=10.5mm. (d) Experiment 4:Q=540g/h and e=12.9mm

3.3.2. Concentration distribution of tetralin in the autoclave

Fig. 11 shows the drying evolution over time. Mass fraction contours of tetralin are plotted at different times with the second approach (penetrable gel). Areas with the highest tetralin concentration are marked with red color, lowest with blue color. These contours show that the tetralin concentration in the fluid surrounding the gel is close to zero $C_\infty \approx 0$. This indicates that the tetralin extracted from the gel leaves immediately the autoclave with the fluid CO_2 exiting from the extractor. A maximal concentration zone is observed in the gel center. The organogel sample is dried progressively from the sides to the center. Over time, the zone of high concentration is reduced and the tetralin concentration decreases in the whole gel. This evolution is similar to that observed by Lebedev *et al.* [36] during silica gel drying. It is clear also that the removal of the tetralin from the gel volume mainly takes place during the first 50 min of the process.

Initial time of drying t = 100s

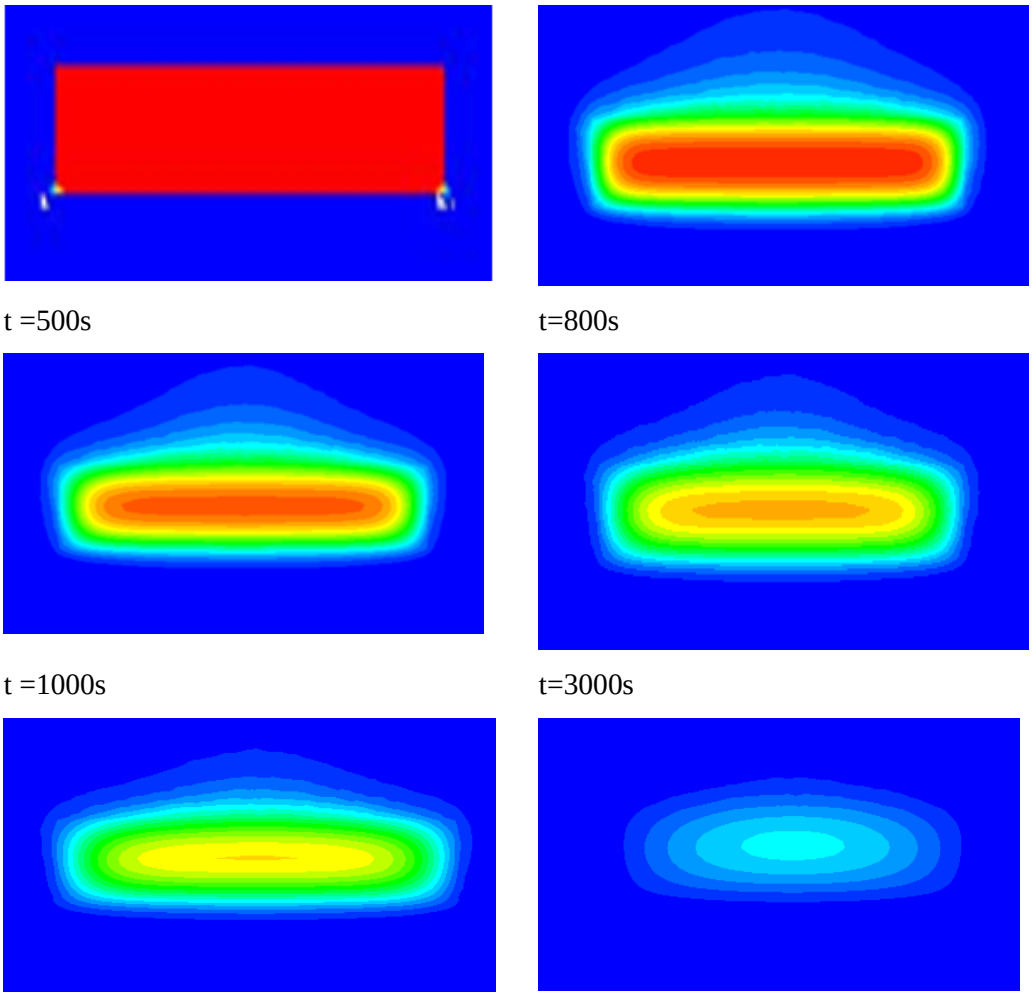

Fig. 11. Contours of tetralin mass fraction at the central section vertical to the autoclave at different time, zoomed around the sample (experiment 1).

3.3.3. Parametric study

A parametric study is also performed to determine the sensitivity of the drying kinetic to variables such as $SCCO_2$ flow rate and gel thickness using the second approach.

The effect of $SCCO_2$ flow rate on the drying kinetics of a 6.7mm-height, 30mm-diameter organogel sample at 45°C and 180 bar is examined using a wide range of CO_2 flow rate between 100g/h and 1700 g/h, that includes the experimental flow rates. The tetralin mass fraction in the organogel as a function of time is converted into recovery rate of removed from the pores with drying time (Eq 10). **Fig.12** indicates how the tetralin recovery rate evolves with time for various flow rates. An increasing flow rate of $SCCO_2$ leads to a decrease of the effluent concentration and consequently to a decrease of the drying time. The different simulations demonstrate that a significant effect is observed on drying for flow rates in the range 100g/h and 1700g/h. A similar conclusion was also reached by a similar study by

Lebedev *et al.*[36] which was recently published. These results should be confirmed with experiments to conclude that for industrial scale, it is necessary to run at a high CO_2 flow rate in order to minimize drying time. But also, an optimal CO_2 flow rate should be evaluated because a very high CO_2 flow rate can lead to cracking of the organogel sample as it is observed experimentally.

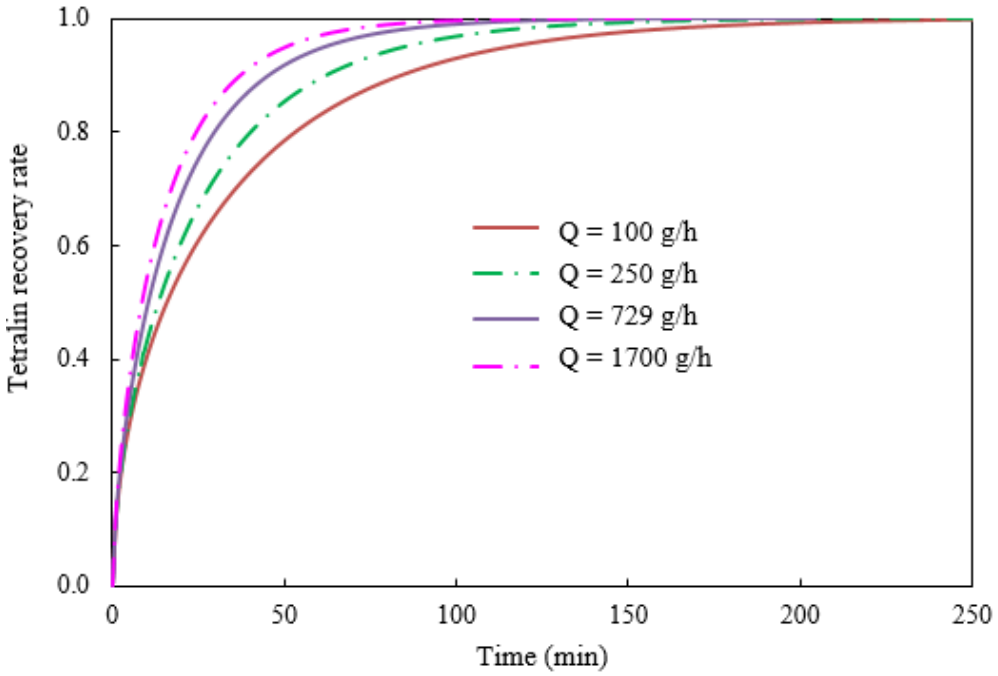

Fig.12. Variation of tetralin recovery rate as a function of time at varying $SCCO_2$ mass flow rate at 180 bar and 45°C, with a 30 mm sample diameter and a 6.7 mm sample height.

Organogel thickness is one of the most important parameters influencing drying time. Effect of gel thickness on drying kinetic is evaluated by performing simulations for organogel samples with 30mm diameter and with heights of 6.7 mm, 10.5 mm and 12.9 mm. The drying conditions are 45°C and 180 bar with a $SCCO_2$ flow rate of 729g/h. The simulations results are plotted in **Fig. 13**. As expected and as is concluded in a similar study [35] thicker organogel samples need longer drying times. The CO_2 which penetrates into the gel follows a longer path as the gel sample thickness increases. The drying time increases from 135 to 210 min as the height increases from 6.7mm to 12.9 mm. Both the $SCCO_2$ flow rate and the gel thickness have important effects on the drying kinetics.

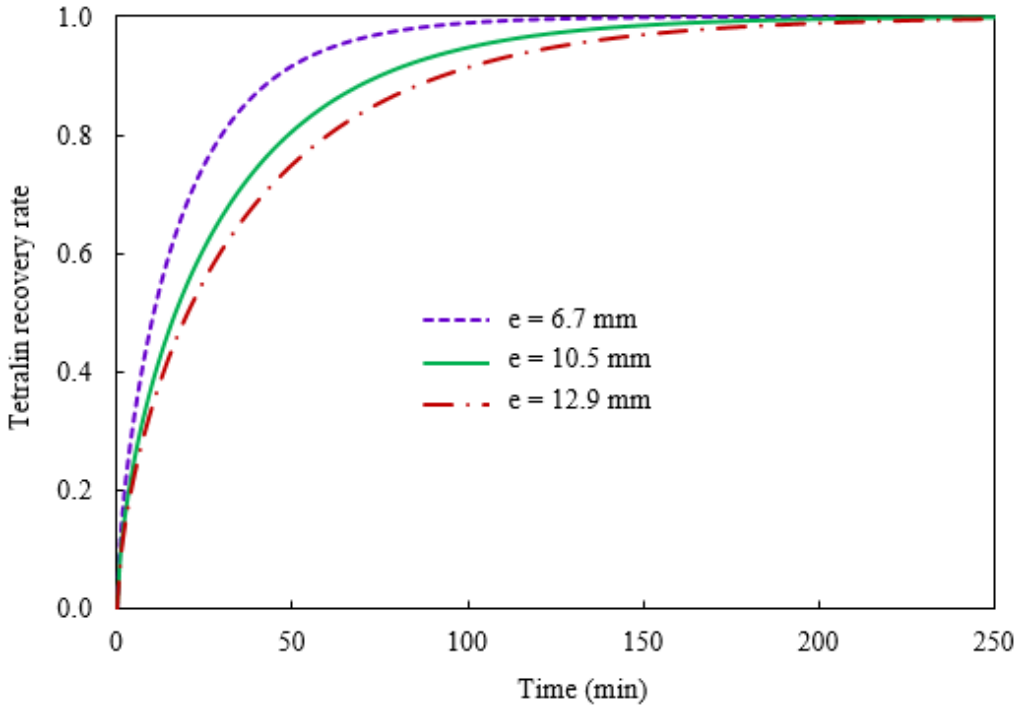

Fig. 13. Variation of tetralin recovery rate as a function of time at varying organogel thickness (6.9mm, 10.5mm and 12.9mm) at 180 bar and 45°C and SC-CO2 flow rate of 729 g/h

4. Conclusion

In order to investigate the supercritical drying process of organogel for aerogels production, both experimental and theoretical studies have been carried out. The experiments have been performed in a supercritical pilot unit. Different samples of 30 mm diameter and 6.7mm to 12.9 mm thickness were dried with a supercritical CO_2 stream in an autoclave at 45°C and 180 bar. Based on the previsions of continuum mechanics, two mathematical models have been established to describe the hydrodynamics of the CO_2 flow and mass transfer of solvent during drying process. In a first approach, the organogel was considered as an impenetrable sample. Mass transfer in the gel was described by Fick diffusion, with an effective diffusivity to account for the gel porosity. In a second approach, the organogel was regarded as penetrable by the CO_2 flow. In this case, convective transport occurred together with diffusion. For both models, the molecular diffusion coefficient, the diffusivities, gel and glass beads permeabilities were estimated from literature correlations. The numerical results, tetralin recovery rate as function of time, of both models were compared to experimental data. The second model, in which the gel was considered as penetrable, yielded results closer to experiments with relative discrepancies below 20%. This showed that the approach

considering the organogel as a penetrable sample better represents the experimental reality. Using the second approach, many simulations were performed in order to study the effect of CO_2 flow rate and gel thickness, showing a significant effect of both parameters. Likewise, a parametric study with simulations on structural parameters like fibers diameters and solvent hydrodynamic radius would be interesting. It could allow to discriminate the two approaches and investigate the sensitivity of drying kinetics to these parameters.

Acknowledgements

This work was partially supported by the Institut Carnot ICEEL.

References

[1] A. Bisson, A. Rigacci, D. Lecomte, E. Rodier, P. Achard, Drying of Silica Gels to Obtain Aerogels: Phenomenology and Basic Techniques, Dry. Technol. 21 (2003) 593–628.
[2] G.W. Scherer, Freezing gels, J. Non-Cryst. Solids. 155 (1993) 1–25.
[3] L. Durães, M. Ochoa, N. Rocha, R. Patrício, N. Duarte, V. Redondo, A. Portugal, Effect of the Drying Conditions on the Microstructure of Silica Based Xerogels and Aerogels, J. Nanosci. Nanotechnol. 12 (2012) 6828–6834.
[4] S.S. Kistler, Coherent Expanded-Aerogels, J. Phys. Chem. 36 (1932) 52–64.
[5] L.F. Su, L. Miao, S. Tanemura, G. Xu, Low-cost and fast synthesis of nanoporous silica cryogels for thermal insulation applications, Sci. Technol. Adv. Mater. 13 (2012).
[6] B. Jamart-Grégoire, S. Son, F. Allix, V. Felix, D. Barth, Y. Jannot, G. Pickaert, A. Degiovanni, Monolithic organic aerogels derived from single amino-acid based supramolecular gels: physical and thermal properties, RSC Adv. 6 (2016) 102198–102205.
[7] K. Ganesan, A. Dennstedt, A. Barowski, L. Ratke, Design of aerogels, cryogels and xerogels of cellulose with hierarchical porous structures, Mater. Des. 92 (2016) 345–355.
[8] S. Reichelt, J. Becher, J. Weisser, A. Prager, U. Decker, S. Möller, A. Berg, M. Schnabelrauch, Biocompatible polysaccharide-based cryogels., Mater. Sci. Eng. C Mater. Biol. Appl. 35 (2014) 164–170.
[9] F. Shi, L. Wang, J. Liu, Synthesis and characterization of silica aerogels by a novel fast ambient pressure drying process, Mater. Lett. 60 (2006) 3718–3722.
[10] Y. Masmoudi, A. Rigacci, P. Achard, F. Cauneau, Supercritical CO2 drying of silica aerogels synthesized in 2-propanol, in: 7th Ital. Conf. Supercrit. Fluids Their Appl. 9th Meet. Supercrit. Fluids, 2004: p. 12.
[11] B.M. Novak, D. Auerbach, C. Verrier, Low-Density, Mutually Interpenetrating Organic-Inorganic Composite Materials via Supercritical Drying Techniques, Chem. Mater. 6 (1994) 282–286.
[12] R. Saliger, V. Bock, R. Petricevic, T. Tillotson, S. Geis, J. Fricke, Carbon aerogels from dilute catalysis of resorcinol with formaldehyde, J. Non-Cryst. Solids. 221 (1997) 144–150.
[13] H. Tamon, H. Ishizaka, SAXS Study on Gelation Process in Preparation of Resorcinol-Formaldehyde Aerogel, J. Colloid Interface Sci. 206 (1998) 577–582.
[14] S.S. Kistler, Coherent Expanded Aerogels and Jellies, Nature. 127 (1931) 741.
[15] V. Bock, A. Emmerling, J. Fricke, Influence of monomer and catalyst concentration on RF and carbon aerogel structure, J. Non-Cryst. Solids. 225 (1998) 69–73.
[16] M.H. Nguyen, L.H. Dao, Effects of processing variable on melamine–formaldehyde aerogel formation, J. Non-Cryst. Solids. 225 (1998) 51–57.

[17] C. Tan, B.M. Fung, J.K. Newman, C. Vu, Organic Aerogels with Very High Impact Strength, Adv. Mater. 13 (2001) 644–646.
[18] M. Stolarski, J. Walendziewski, M. Steininger, Barbara Pniak, Synthesis and characteristic of silica aerogels, Appl. Catal. Gen. 177 (1999) 139–148.
[19] A. Soleimani Dorcheh, M.H. Abbasi, Silica aerogel; synthesis, properties and characterization, J. Mater. Process. Technol. 199 (2008) 10–26.
[20] L.W. Hrubesh, Aerogel applications, J. Non-Cryst. Solids. 225 (1998) 335–342.
[21] I. Smirnova, P. Gurikov, Aerogels in Chemical Engineering: Strategies Toward Tailor-Made Aerogels, Annu. Rev. Chem. Biomol. Eng. 8 (2017) 307–334.
[22] N. Brosse, D. Barth, B. Jamart-Grégoire, A family of strong low-molecular-weight organogelators based on aminoacid derivatives, Tetrahedron Lett. 45 (2004) 9521–9524.
[23] Q.N. Pham, N. Brosse, C. Frochot, D. Dumas, A. Hocquet, B. Jamart-Grégoire, Influence of the gelator structure and solvent on the organisation and chirality of self-assembling fibrillar networks, New J. Chem. 32 (2008) 1131–1139.
[24] M. Yemloul, E. Steiner, A. Robert, S. Bouguet-Bonnet, F. Allix, B. Jamart-Grégoire, D. Canet, Solvent Dynamical Behavior in an Organogel Phase As Studied by NMR Relaxation and Diffusion Experiments, J. Phys. Chem. B. 115 (2011) 2511–2517.
[25] M.J. van Bommel, A.B. de Haan, Drying of silica aerogel with supercritical carbon dioxide, J. Non-Cryst. Solids. 186 (1995) 78–82.
[26] Z. Novak, Ž. Knez, Diffusion of methanol–liquid CO2 and methanol–supercritical CO2 in silica aerogels, J. Non-Cryst. Solids. 221 (1997) 163–169.
[27] P. Wawrzyniak, Diffusion of ethanol-carbon dioxide in silica gel, J. Non Cryst. Solids. 225 (1998) 86–90.
[28] W. Behr, V.C. Behr, G. Reichenauer, Self diffusion coefficients of organic solvents and their binary mixtures with CO2 in silica alcogels at pressures up to 6MPa derived by NMR pulsed gradient spin echo, J. Supercrit. Fluids. 106 (2015) 50–56.
[29] L.M. Sanz-Moral, M. Rueda, R. Mato, Á. Martín, View cell investigation of silica aerogels during supercritical drying: Analysis of size variation and mass transfer mechanisms, J. Supercrit. Fluids. 92 (2014) 24–30.
[30] J. Quiño, M. Ruehl, T. Klima, F. Ruiz, S. Will, A. Braeuer, Supercritical drying of aerogel: In situ analysis of concentration profiles inside the gel and derivation of the effective binary diffusion coefficient using Raman spectroscopy, J. Supercrit. Fluids. 108 (2016) 1–12.
[31] J. Crank, The mathematics of diffusion, 2d ed, Clarendon Press, Oxford, [Eng], 1975.
[32] M. Mukhopadhyay, B.S. Rao, Modeling of supercritical drying of ethanol-soaked silica aerogels with carbon dioxide, J. Chem. Technol. Biotechnol. 83 (2008) 1101–1109.
[33] A.M. Orlović, S. Petrović, D.U. Skala, Mathematical modeling and simulation of gel drying with supercritical carbon dioxide, J. Serbian Chem. Soc. 70 (2005) 125–136.
[34] J.S. Griffin, D.H. Mills, M. Cleary, R. Nelson, V.P. Manno, M. Hodes, Continuous extraction rate measurements during supercritical CO2 drying of silica alcogel, J. Supercrit. Fluids. 94 (2014) 38–47.
[35] Y. Özbakır, C. Erkey, Experimental and theoretical investigation of supercritical drying of silica alcogels, J. Supercrit. Fluids. 98 (2015) 153–166.
[36] A.E. Lebedev, A.M. Katalevich, N.V. Menshutina, Modeling and scale-up of supercritical fluid processes. Part I: Supercritical drying, J. Supercrit. Fluids. 106 (2015) 122–132.
[37] C.A. García-González, M.C. Camino-Rey, M. Alnaief, C. Zetzl, I. Smirnova, Supercritical drying of aerogels using CO2: Effect of extraction time on the end material textural properties, J. Supercrit. Fluids. 66 (2012) 297–306.

[38] M. Lazrag, D.L. Mejia-Mendez, C. Lemaitre, P.H.E. Stafford, R. Hreiz, R. Privat, A. Hannachi, D. Barth, Thermodynamic and hydrodynamic study of a gas-liquid flow in a cyclone separator downstream supercritical drying, J. Supercrit. Fluids. 118 (2016) 27–38.
[39] M. Lazrag, E. Steiner, C. Lemaitre, F. Mutelet, R. Privat, S. Rode, A. Hannachi, D. Barth, Experimental and thermodynamic comparison of the separation of CO2/toluene and CO2/tetralin mixtures in the process of organogel supercritical drying for aerogels production, J. Sol-Gel Sci. Technol. 84 (2017) 453–465.
[40] F. Allix, Etude Physico-Chimique d'Organogels et d' Aérogels de Faible Poids Moléculaire Dérivés d'Acides Aminés, INPL-Nancy, 2011.
[41] J. Bear, Dynamics of Fluids in Porous Media, Courier Corporation, New York, 1972.
[42] R.P. Dias, C.S. Fernandes, M. Mota, J.A. Teixeira, A. Yelshin, Permeability and effective thermal conductivity of bisized porous media, Int. J. Heat Mass Transf. 50 (2007) 1295–1301.
[43] R.P. Dias, C.S. Fernandes, J.A. Teixeira, M. Mota, A. Yelshin, Permeability analysis in bisized porous media: Wall effect between particles of different size, J. Hydrol. 349 (2008) 470–474.
[44] M. Mota, J.A. Teixeira, W.R. Bowen, A. Yelshin, Binary spherical particle mixed beds : porosity and permeability relationship measurement, (2001).
[45] L. Zhou, C. Erkey, A. Akgerman, Catalytic oxidation of toluene and tetralin in supercritical Carbon Dioxide, AIChE J. 41 (1995) 2122–2130.
[46] I. Medina, Determination of diffusion coefficients for supercritical fluids, J. Chromatogr. A. 1250 (2012) 124–140.
[47] B. Amsden, Solute diffusion in hydrogels: an examination of the retardation effect, Polym. Gels Netw. 6 (1998) 13–43.
[48] L. Masaro, X.X. Zhu, Physical models of diffusion for polymer solutions, gels and solids, Prog. Polym. Sci. 24 (1999) 731–775.
[49] A.G. Ogston, B.N. Preston, J.D. Wells, On the Transport of Compact Particles Through Solutions of Chain-Polymers, Proc. R. Soc. Math. Phys. Eng. Sci. 333 (1973) 297–316.
[50] A.G. Ogston, The spaces in a uniform random suspension of fibres, Trans. Faraday Soc. 54 (1958) 1754.
[51] R.M. Davies, G. Taylor, The Mechanics of Large Bubbles Rising through Extended Liquids and through Liquids in Tubes, Proc. R. Soc. Lond. Math. Phys. Eng. Sci. 200 (1950) 375–390.
[52] K.M. de Reuck, B. Armstrong, International thermodynamic tables of the fluid state: carbon dioxide, Pergamon Press, Oxford; New York, 1976.
[53] A. Fenghour, W.A. Wakeham, V. Vesovic, The Viscosity of Carbon Dioxide, J. Phys. Chem. Ref. Data. 27 (1998) 31–44.
[54] A. Bondi, van der Waals volumes and radii, J. Phys. Chem. 68 (1964) 441–451.
[55] H. Rumpf, A.R. Gupte, The influence of porosity and grain size distribution on the permeability equation of porous flow, Chem. Ing. Tech. 43 (1975) 367–375.